


**Slow dynamics in a single bead with mechanical conditioning and transient heating**Richard L. Weaver<sup>1</sup> and SangMin Lee<sup>2</sup><sup>1</sup>*Department of Physics, University of Illinois Urbana-Champaign, Urbana, Illinois 61801, USA*<sup>2</sup>*Department of Civil and Environmental Engineering, University of Illinois Urbana-Champaign, Urbana, Illinois 61801, USA* (Received 27 June 2022; revised 28 November 2022; accepted 17 March 2023; published 24 April 2023)

The contact stiffness of an aluminum bead confined between two slabs diminishes upon mechanical conditioning, and then recovers as  $\log(t)$  after the conditioning ceases. Here that structure is evaluated for its response to transient heating and cooling, with and without accompanying conditioning vibrations. It is found that, under heating or cooling alone, stiffness changes are mostly consistent with temperature-dependent material moduli; there is little or no slow dynamics. Hybrid tests in which vibration conditioning is followed by heating or cooling lead to recoveries that begin as  $\log(t)$  and then become more complex. On subtracting the known response to heating or cooling alone we discern the influence of higher or lower temperatures on slow dynamic recovery from vibrations. It is found that heating accelerates the initial  $\log(t)$  recovery, but by an amount more than predicted by an Arrhenius model of thermally activated barrier penetrations. Transient cooling has no discernible effect, in contrast to the Arrhenius prediction that it slows recovery.

DOI: [10.1103/PhysRevE.107.044902](https://doi.org/10.1103/PhysRevE.107.044902)**I. INTRODUCTION**

Natural rocks and cements exhibit remarkable and seemingly universal nonclassical nonlinear elastic behaviors. Among those is slow dynamics (SD), in which a modest mechanical conditioning strain induces a loss of stiffness that afterward recovers, slowly, as  $\log(\text{time})$ . The SD stiffness loss and slow recovery are not comprehended within classical nonlinear elasticity. Inasmuch as the stiffness depends on the history of stress it is a peculiar species of time-dependent nonlinear elasticity. This apparent healing after damage is seen in many materials, on length scales from the laboratory to the seismic, and on timescales from milliseconds to years. Laboratory applications of minor strain (as little as  $10^{-6}$ ) lead to drops in elastic modulus that then slowly recover [1–9]. Loss of stiffness and slow recovery are seen also in seismic wave speed near a fault after an earthquake [10–12] where recoveries are monitored over periods from days to years. SD is observed in concrete and mortar [13,14] and in buildings [15]. Shokouhi *et al.* [8] and Kober *et al.* [16] report intriguing deviations from  $\log(t)$ .

SD behavior is not confined to rocks and cements. Materials with simpler chemistry and structure show the effect as well. Bittner and Popovics [17,18] showed that a glass block under impact conditioning exhibited slow dynamics after it was thermally cracked, but not before. Zaitsev *et al.* [19] observed slow dynamics in thermally cracked glass rods. Slow dynamic nonlinearity is also found in unconsolidated materials; it has been observed in aggregates of spherical glass beads under static load, by Johnson and Jia [20] who posited a connection to dynamic earthquake triggering, by Zaitsev *et al.* [21], by Jia *et al.* [22], and by Yoritomo and Weaver [23]. The latter observed slow dynamics in a single bead confined between two plates [24] and among glass, aluminum, and steel beads [25]. The inference is that unconsolidated materials replace slow dynamic processes at the internal intergrain

contacts of rocks with processes taking place at bead contacts. Rocks and cements have complex and varied internal structures and chemistries that present corresponding challenges in identifying microphysical mechanisms. However, the presence of SD in simpler materials and the apparent universality across so many natural materials and cements [6,26], and in both metals and insulators, suggests that the microphysical mechanism is simple and common, leading to hopes that it can be understood on a universal basis.

Conditioning need not be mechanical. Ten Cate *et al.* report [27] modulus loss and slow recovery following imposed changes of temperature. Figure 1 shows initial drops in the modulus (here represented in terms of a resonant frequency), followed by an hours-long rise. In the case of a temperature decrease [Fig. 1(a)], the initial drop is small and the later rise is large, eventually leaving the material with a net increased stiffness, consistent with the usual case that the modulus rises after a temperature decrease. Figure 1(b) shows the opposite: a large initial drop followed by a slow and modest rise over hours that leaves a net decrease in the modulus at late times.

SD drops in resonant frequencies are associated with increases in loss rates. Johnson and Sutin [6] in a survey of a number of materials found changes in inverse quality factor  $Q$  to be proportional to the change in resonant frequency  $\omega$  by

$$\Delta Q^{-1}/Q^{-1} = -\gamma_{\text{SD}}[\Delta\omega/\omega]Q, \quad (1)$$

with coefficient  $\gamma_{\text{SD}}$  varying from 0.23 to 0.46 among different materials. Inasmuch as  $Q$  is typically large,  $Q \gg 1$ , the fractional change in  $Q$  is typically much greater than the fractional change in resonant frequency.

Closely related are studies of anomalous nonlinear fast dynamics [5,6,28] in which these materials also show a nonclassical nonlinearity under sinusoidally imposed stresses. Lebedev and Ostrovsky [29] have a model in which both fast and slow dynamics are comprehended within a single unified

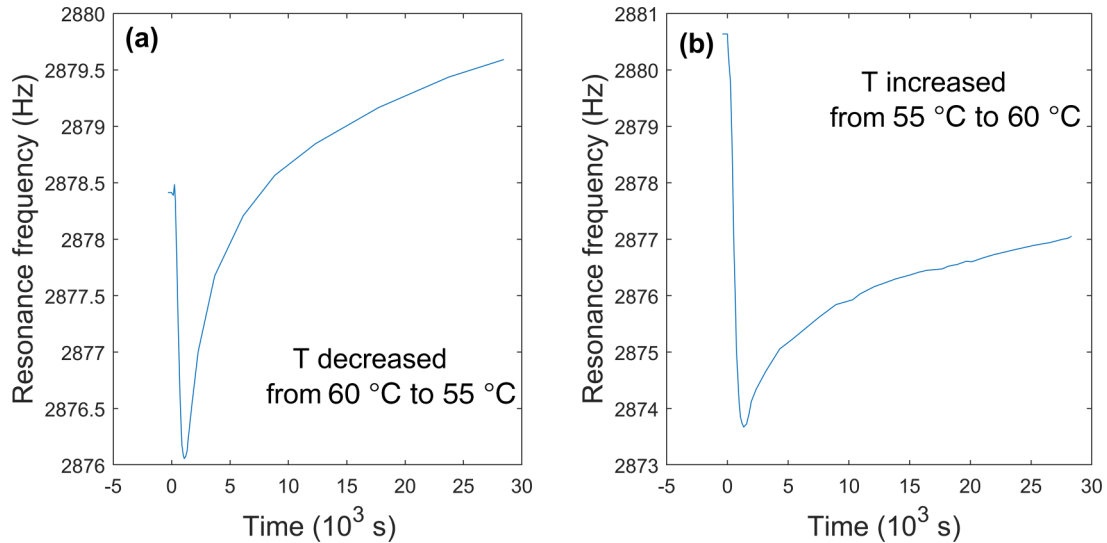


FIG. 1. Variation of a sandstone prism’s resonant frequency when (a) temperature is dropped by 5 °C and (b) when temperature is increased. In both cases stiffness drops quickly and then rises slowly. At late times the stiffness is (a) greater or (b) less than its starting value. Data taken from Ten Cate *et al.* [27].

microphysical mechanism. Sens-Schoenfelder *et al.* [30] propose a phenomenological set of local stress-strain relations that, after parameters are chosen, produce the detailed fast dynamic behavior observed by Renaud *et al.* [28] and slow dynamic recoveries.

There remains no consensus as to the mechanisms responsible for SD. Among the speculations there are a few chief, though not exclusive, hypotheses. One is that moisture plays a critical role. This is supported by the well accepted dependence of rock moduli on the presence of trace amounts of moisture, and by observations of humidity sensitivity for SD in cracked glass [17,18] and humidity sensitivity of fast dynamic nonlinearity in an unconsolidated granular medium [31]. It is also suggested by Bouquet *et al.*’s observation [32] of  $\log(t)$  aging, and humidity dependence of the strength of a sand pile against avalanching, and their model of the aging as due to thermal activation of nanoscopic water bridges. Another hypothesis may be termed “the Arrhenius,” for which recovery proceeds [1,29,33] due to thermally activated barrier penetration and bond formation, and for which details are presented below. A variation connects the widely observed logarithmic aging of static friction strength with the logarithmic SD aging of stiffness. Baumberger and Caroli [34] show in their review of solid friction that (1)  $\log(t)$  aging of frictional strength is observed over a wide range of materials and (2) it is observed in the growth of contact areas, and (3) it may be derived theoretically from a model of plastic creep if the rate thereof is governed by a model in which plastic strain rate is, Arrhenius-like, exponential in the ratio of stress to temperature [35]. It is highly plausible that the growth of the contact asperity area would lead to both static friction strengthening and to the increasing stiffness observed in the SD literature.

The Arrhenius picture is prevalent among hypotheses for the mechanisms of SD. Yet tests to date [1] have been unable to confirm the predicted absolute temperature proportionality of the  $\log(t)$  recoveries. As discussed below, however,

tests that combine time-varying temperature with mechanical conditioning may prove more sensitive than those at fixed temperature.

The work reported here is part of an experimental program whose intent is to elucidate the mechanisms behind these non-classical behaviors. The next section provides an overview of our single-bead experimental setup and the SD measurements that are conducted there. This is followed in Sec. III on the response of the single-bead system to transient temperature changes. Stiffness changes due to heating or cooling are found to be mostly consistent with the familiar sensitivity of moduli to temperature, with minor contributions from SD; the behavior (Fig. 1) seen by Ten Cate *et al.* [27] is not reproduced.

In order to investigate the Arrhenius hypothesis and thermal activation, Sec. IV then presents measurements of SD in hybrid tests involving combinations of vibration conditioning and transient heating. It is found that heating accelerates SD recovery from vibration conditioning, but does so more strongly and with more permanence than is predicted by the Arrhenius hypothesis. Transient cooling has no effect on healing. Section V summarizes our conclusions.

## II. OVERVIEW OF SINGLE-BEAD EXPERIMENTS

Figure 2 sketches our laboratory system. A 3 mm diameter aluminum bead is confined between two aluminum slabs (dimensions: 215 mm long  $\times$  155 mm wide  $\times$  19 mm thick). Optional heating is applied to the blackened face of the bead by a continuous wave 450 nm diode laser. Bead temperature is monitored by a thermocouple with a noise level of  $\pm 0.01^\circ\text{C}$ . A high voltage pulse is applied to the piezoelectric transducer on the upper slab. The resulting ultrasound reverberates in the upper slab and slowly diffuses into the lower slab by way of natural modes of vibration of the confined bead. The transmitted ultrasound is dominated by a band of frequencies 90–110 kHz. Changes in the signal received in the lower slab indicate changes in the modes’ resonant frequencies, and thus

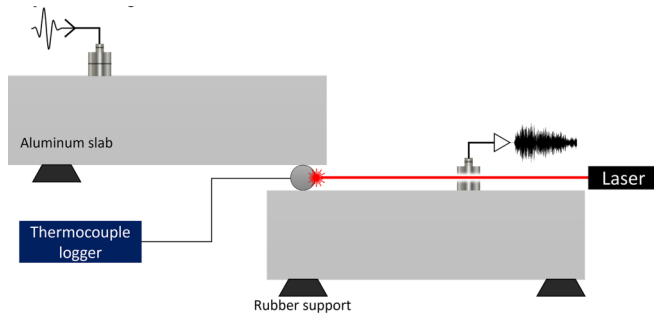


FIG. 2. A not-to-scale sketch of the laboratory measurement system. A 3 mm diameter aluminum bead is confined between aluminum slabs instrumented with piezoelectric ultrasound transducers. The bead’s resonant frequencies depend on the stiffness of the bead-slab contact, diminishment in which manifest as delays of the transmitted waveform.

of changes in material elastic moduli or other contributions to contact stiffness. Conditioning is applied by an electromagnetic shaker (not shown) acting on the base. The entire structure sits on a vibration isolation platform and an optical table to shield it from ambient vibrations. With negligible exceptions (see below), the slabs remain at ambient temperature throughout all tests.

Changes in the diffuse waveform received in the lower slab are analyzed using coda wave interferometry [24,36,37]. These measurements differ from others in the SD literature that typically quote frequency or modulus changes. Here the measured parameter is a time shift. Delays or advances,  $Y$ , in the transmitted diffuse signal are detected with nanosecond precision. Weaver and Lee [37] showed that  $Y$  is related to the bead’s resonant frequency changes by  $Y = (\Delta\omega/\omega)$  times a random time-independent function  $R$  of the system geometry

and bead position inherited from the stochastic nature of the reverberant diffuse fields with unity mean  $\langle R \rangle = 1$ , times a “dwell time”  $1/2\gamma$  defined as the average lifetime of bead vibration energy as it decays due to absorptive or radiative losses.

$$Y = [\Delta\omega/\omega]R/2\gamma = [\Delta\omega/\omega][R/\omega]Q. \quad (2)$$

The bead’s free vibration amplitude loss rate  $\gamma = \omega/2Q$  is not to be confused with  $\gamma_{SD}$ . Examples of  $Y$ ’s measurement, and diminishment and slow recovery after mechanical conditioning, are given by Weaver and co-workers [24,25,37].

$Y$  is constructed to be insensitive to gross temperature changes in the structure. Slab heating will indeed delay a diffuse waveform, and will do so proportionally to the travel time of the waves; waves with greater travel time experience proportionally more temperature-induced delay [37], but  $Y$  is constructed [24,37] as the zero-travel-time limit of the delays and is thereby unaffected by slab temperature changes, if any.

Figure 3 shows three measurements of  $Y$  separated by 60 min, each covering a period before, during, and after 30 s of vibration conditioning. The bead temperature is constant. The laser remains off. A mechanical shaker attached to the optical table upon which the slabs sit is driven at 500 Hz. Acceleration amplitudes of the upper slab during conditioning are typically  $1 \text{ m/s}^2$ . This corresponds to rms strain across the bead of about  $64 \mu\text{strain}$ . The diffuse time shift  $Y$  (negative values correspond to delays) of a given received ultrasonic waveform is evaluated relative to a reference waveform recorded at a time shortly before the most recent vibration conditioning began. During the vibration  $Y$  is irregular and not meaningful. After the vibration ceases,  $Y$  is negative, thus representing diminishment of contact stiffness. In all cases the delays then recover and, as seen in Fig. 3, do so with the same slope:  $dY/d\ln(t) \sim 31 \text{ ns}$ . Linearity vs  $\ln(t)$  is striking. The three recoveries differ in offset but are otherwise repeatable, the first

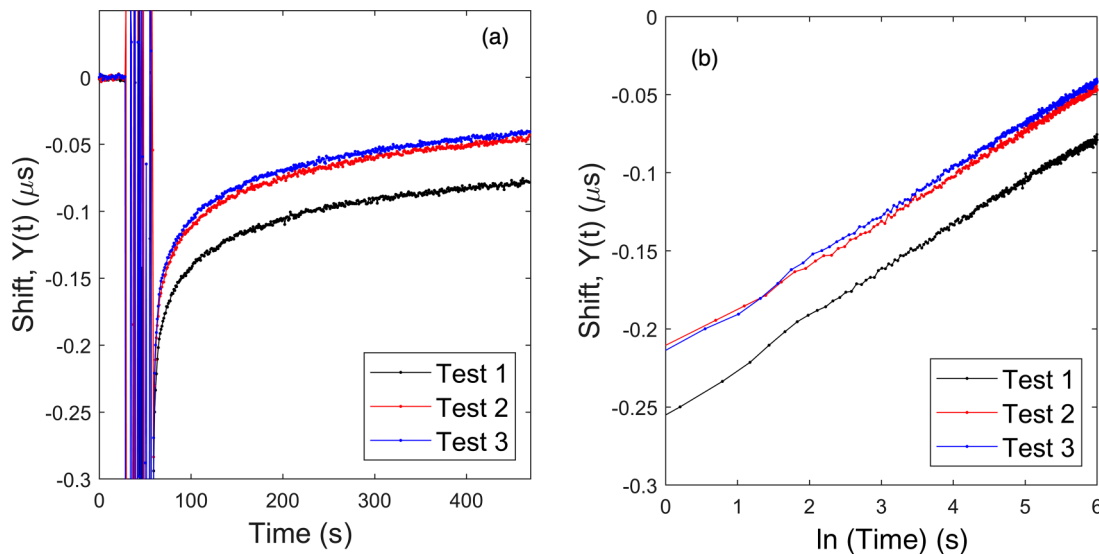


FIG. 3. Diffuse field shifts  $Y(t)$  for successive tests separated by 60 min: (a) plotted vs time, (b) plotted vs  $\ln(\text{time})$ . The results of the first test are indicated in the lower, black, line; the middle red line and upper blue line pertain to the second and third tests respectively. Negative values of  $Y$  correspond to delays of ultrasound on passing through the bead, i.e., to diminishment of stiffness. These data constitute an example of vibration-induced loss of stiffness followed by slow, logarithmic recovery. rms noise in  $Y$  is of the order of a couple of nanoseconds. The noise is attributed to building vibrations and has been reduced by the use of vibration isolation tables.

vibration (test 1) causing a greater delay than the others. This is because each test's  $Y$  is measured relative to the system state just before that test's vibration, yet each conditioning leaves the system with the same absolute stiffness. The difference in offset reflects the healing that has happened since previous tests. Except for the offset, repeatability is good as long as the bead is undisturbed.

Plotting vs  $\ln(t - t_0)$ , or construction of relaxation spectra [8,26], can be ambiguous, as one must choose a reference time,  $t_0$ . It would be natural to set this at the time when conditioning vibrations cease, but no vibration ceases instantaneously, so the appropriate value is unclear. Fortunately the choice only affects the plots at short times,  $\log(t) < 1$ . Because of this insensitivity and because vibration was not monitored *vis-à-vis* the ultrasonic pulses, here all plots take  $t_0$  from the 1 s interval between the time of the last reported datum still clearly affected by the ongoing vibrations where  $Y$  is not meaningful and the next recorded  $Y$ . The precise value is chosen such that the plots are rendered as linear as possible. That is admittedly a convenient choice. In practice different choices only affect the first couple of points, data points that are unimportant to the present purposes. Separate, more recent studies (not shown) with  $Y$  evaluated approximately every 70 ms, with simultaneous evaluation of the conditioning slab acceleration  $A(t)$ , and  $t_0$  chosen to coincide with the beginning of  $A(t)$ 's cessation, show that  $Y$  vs  $\log(t)$  maintains good linearity above 50 ms, and excellent linearity for  $t$  above 1/3 s, thus justifying the otherwise *ad hoc* choice here of  $t_0$  that gives best linearity. The interesting tangential issue of whether and where there may be significant deviations from linearity [8,16] below 50 ms cannot be addressed with this structure.

The work reported here includes tests with laser heating, as illustrated in Fig. 2. A blue-green 450 nm nominal 1 W continuous wave diode laser is focused on the front face of the bead, typically for 30 s. The resulting temperature rise of the bead leads to heat flow across the interfaces and into the slabs, thereby limiting the rise of bead temperature to a steady state, in Fig. 4 at about 12.5 °C. Simple heat conduction arguments predict that the steady state temperature increase at the interfaces is half that of the bead. They also establish that there is a region of inhomogeneous temperature and high heat flux confined to near the interface over a length scale provided by the radius of the contact,  $\sim 47 \mu\text{m}$ . We calculate that the longest time constant for heat flow within a bead is  $1/k^2d = 0.006$  s and effectively instantaneous. Here  $d = 93 \text{ mm}^2/\text{s}$  is the heat diffusivity in aluminum,  $\kappa = z/a$  where  $a$  is the bead radius, and  $z$  is the first zero of the slope of the spherical Bessel function:  $j'_i(z) = 0$ ;  $z = 2.07$ . Other calculations establish that 1 W of heating of 3 kg of aluminum for 30 s will raise its temperature by no more than 0.01 °C, and less than that if heat flow to the air is considered, so the slabs are not appreciably heated during tests.

### III. MEASUREMENTS OF TEMPERATURE AND CONTACT STIFFNESS CHANGES ON TRANSIENT HEATING AND COOLING

Here we report the bead's responses, both in temperature and stiffness, to heating and cooling. It is found that changes in contact stiffness, as manifested in shifts  $Y$ , are consistent

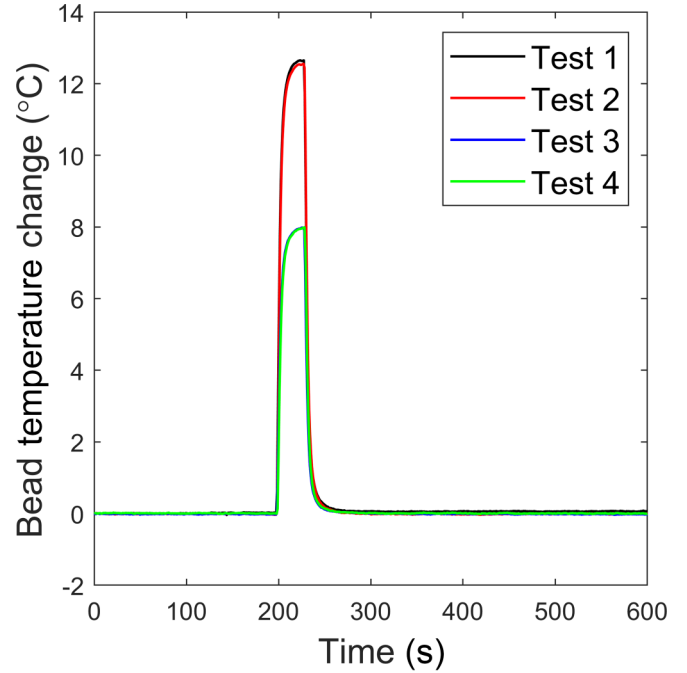


FIG. 4. The bead temperature, relative to its initial value and to the slab temperature, for cases in which the laser is on for 30 s. Tests 3 and 4 are at a lower laser intensity. Consistency is good. Peak values for temperature change, here about 12.5 °C, are observed to vary with bead repositioning, possibly due to repositioning affecting optical absorptivity or bead-slab thermal conductance.

with a simple picture in which  $Y$  is dominated by a proportionality to bead temperature changes,  $Y = \beta T_b$ . Deviations are present but weak; there are no significant nonlinear or delayed or SD effects. Tests are conducted with both transient heating and transient cooling. All bead and interface temperatures are reported as changes relative to the temperature immediately before any heating or cooling, unless otherwise indicated. In the case of transient heating (Sec. III A) this is the same as relative to the slab.

#### A. Transient heating

Figure 4 shows the temperature change  $T_b(t)$  of the single bead, as reported by the thermocouple before, during, and after 30 s of laser heating. Four measurements are shown in order to illustrate repeatability, the indistinguishable third and fourth with lower laser power.

The rise and fall fit well to a model of linear conductance in which bead temperature relative to that of the slabs, and to initial bead temperature, is  $T_b(t) = (\tau \Pi_0 / C)[1 - \exp(-t/\tau)]$  while the laser is on. Here  $C$  is the bead's heat capacity and  $\Pi_0$  is the thermal power being deposited by the laser. The model predicts  $T_b(t) = T_0 \exp(-t/\tau)$  for times after the laser is turned off. The time constant  $\tau$  is given by  $C/2\alpha$  where  $\alpha$  is the conductance between bead and slab in Watts per unit temperature difference across the interface. The data fit well with a time constant  $\tau$  of 3.2 s, for both heating and cooling, and for both high and low laser power. It is curious that a model in which the interface is a uniform pancake of radius 47  $\mu\text{m}$  (based on Hertzian contact theory [38]) predicts [38]



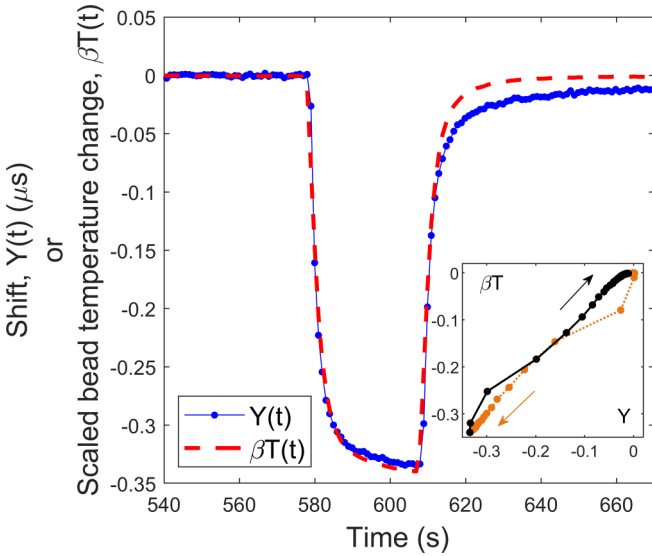


FIG. 5. For a laser-on duration of 30 s,  $Y(t)$  (blue dots) is compared to  $\beta T_b(t)$  (red dashed curve) with a best fit  $\beta$  of  $-0.0310 \text{ ms}/^\circ\text{C}$ .  $Y(t)$  for laser heating is close to proportional to bead temperature  $T_b(t)$ , thus indicating that  $Y$  is dominated by linear elasticity with temperature-dependent moduli. At late times  $t > 620 \text{ s}$  there is a residual loss of stiffness not encompassed by  $\beta T$ . The inset shows  $Y$  vs  $\beta T_b$  and illustrates the degree to which proportionality is imperfect, in particular, that there are weak deviations discernible even before the final relaxation. Arrows indicate directions of increasing time.

a conductance  $\alpha$  such that  $\tau = 0.76 \text{ s}$ . Our measurement of  $3.2 \text{ s}$  indicates that heat conduction is impeded by complexity at the interface. One imagines oxide layers, moisture, or air gaps as playing roles. That the time constants of the tests at high and low laser intensity in Fig. 4 are the same suggests that nonlinearities are unlikely to explain the curiously low thermal conductance at the interfaces. The literature [39] has it that the net conductance across a highly imperfect contact scales with the sum of the radii of many small well separated contacts rather than the apparent radius of the entire region. A more precise theory may thus predict a conductance much less than the simple estimate.

Figure 5 shows the shift  $Y(t)$  for 30 s of laser heating.  $Y(t)$  is compared to  $\beta T_b(t)$  with a best fit  $\beta = -0.031 \text{ } \mu\text{s}/^\circ\text{C}$ , showing that  $Y$  is approximately simply proportional to bead temperature.  $\beta$  was chosen to minimize the mean square deviation between  $\beta T_b$  and  $Y$ :  $\sum_i [Y(t) - \beta T_b(t)]^2$ . Points are equally weighted. For these plots of  $T$  and  $Y$  we have corrected for time delay  $\Delta$  between plots of  $T$  and  $Y$  which is reported by the thermocouple [40],  $T_b(t) = T_{\text{thermocouple}}(t + \Delta)$ . By close analysis of the quickest of  $T$  and  $Y$  changes (for both the cooling and heating protocols, in Figs. 5 and 6, respectively),  $\Delta$  has been determined to be  $0.6 \text{ s}$ . As seen in the plot, shifts  $Y(t)$  fit well to  $\beta T_b(t)$ , but not exactly. Residual stiffness loss is apparent in Fig. 5 at late times,  $t > 620 \text{ s}$ , even after the temperature has dropped back to zero. The residual stiffness loss peaks at about 20 ns, 15 s after laser-off, but drops to about 10 ns at a point 50 s after laser-off. It recovers slowly in a manner reminiscent of slow dynamics. The dynamic range covered by recovery is

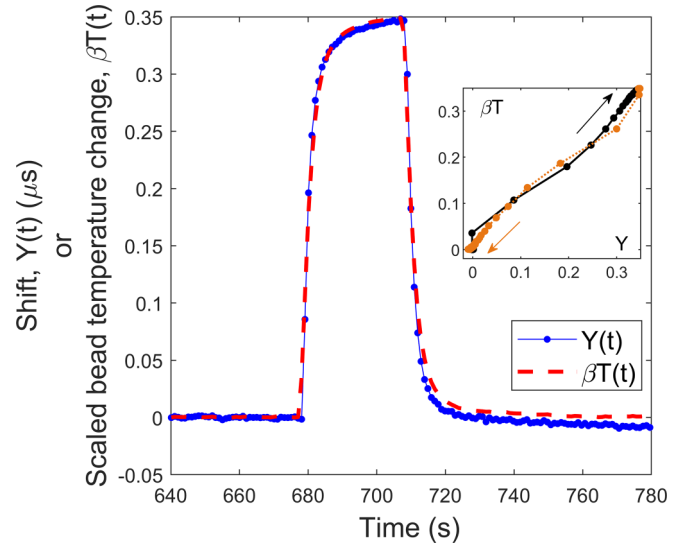


FIG. 6.  $Y$  for a case of transient cooling is compared to scaled bead temperature. Best fit  $\beta$  was  $-0.0316 \text{ } \mu\text{s}/^\circ\text{C}$ . A weak stiffness loss persists at late times and shows no sign of relaxing yet. An inset showing  $Y$  vs  $\beta T_b$  illustrates the degree to which proportionality is imperfect. Arrows indicate directions of increasing time.

sufficiently low, and the ambiguities as to choosing a reference time with which to define  $\ln(t)$  are sufficiently great, that we cannot clearly identify it as logarithmic. The inset of Fig. 5 shows  $\beta T$  vs  $Y$ , with indications that differences between  $Y$  and  $\beta T$  are also present before laser-off.

As discussed above, the slabs are not appreciably heated by the laser. They remain at ambient temperature except for a small region near the bead interfaces where slab temperature falls away from  $T_b/2$  to zero (relative to initial, i.e., ambient, i.e., slab), for distances  $r > a$ , like  $a/r$  where  $a$  is of the order of the contact radius and about  $47 \text{ } \mu\text{m}$ .

$Y(t) = \beta T_b(t)$  would be predicted by a model in which there are no heating-induced structural changes or broken bonds and no slow dynamics, and in which the material moduli in the vicinity of the interface vary linearly with temperature. To see this and to construct a theoretical estimate for  $\beta$  we first recall that the bead-slab contact stiffness, as calculated by Hertzian elastic contact theory [38,24], varies with the  $2/3$  power of the Young's modulus  $E$  in the vicinity of the contact. In consequence the resonant frequencies  $\omega$  then vary with the  $1/3$  power of  $E$ .  $E$  in aluminum varies with temperature as  $\delta E/E = \mu \delta T$ , with  $\mu = -5.3 \times 10^{-4}/^\circ\text{C}$  [41]. Contact stiffness also depends on Poisson ratio and on the radius of the bead, but we neglect those quantities as less important. We note that the temperature  $T_i$  in the vicinity of the interface is half the temperature  $T_b$  of the bead ( $T_b$  and  $T_i$  are defined relative to their initial values, i.e., the temperature of the slab) and conclude that  $\Delta\omega/\omega = (\mu/6)T_b$  where  $\omega$  is a bead's resonant frequency. We then recall [Eq. (2)] that  $Y = R[\Delta\omega/\omega]/2\gamma$ . Putting these estimates together predicts  $Y = \beta T_b$  with  $\beta = R\mu/12\gamma$ . This model for temperature dependence in  $Y$  ignores any nonclassical elasticity, and in particular any slow dynamics. It is furthermore uncertain to the degree that attenuation  $\gamma$  and the random  $R$  are unknown, but it nevertheless provides a comparison for measurements.

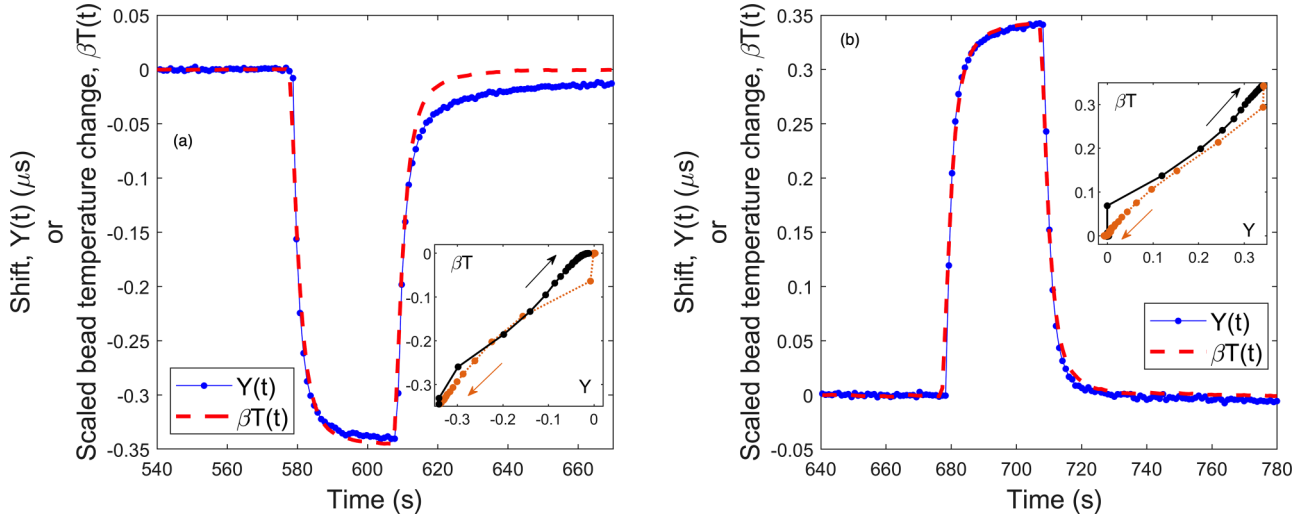


FIG. 7. The behaviors exhibited in Figs. 5 and 6 are reproduced in separate measurements on the same bead: (a) for heating and (b) for cooling. Here best fit  $\beta$  is  $-0.0313$  for both cases. Time delays between bead temperature and thermocouple reading remain at  $\Delta = 0.6$  s.

It is emphasized that this contribution to the temperature dependence of  $Y$  is classical; it includes only the effects of the temperature dependence of aluminum's Young's modulus in the vicinity of the contact.

Figure 5's fit is remarkably good considering the simplicity and linearity of the theoretical picture. The best fit  $\beta$  in Fig. 5 is  $-0.031 \mu\text{s}/^\circ\text{C}$ , but varies with bead repositioning. We have observed values from  $-0.02$  to  $-0.045 \mu\text{s}/^\circ\text{C}$ , a variation that indicates the influence of the stochastic variable  $R$  and suggests a best guess for  $\gamma$  in the vicinity of  $1400/\text{s}$ , corresponding to a quality factor  $Q = \omega/2\gamma$  of about 220, comparable with previous estimates [37].

### B. Transient cooling

A similar test is illustrated in Fig. 6, conducted on the same undisturbed bead, but now with a laser protocol that emulates transient *cooling*. The test begins with a laser-on duration of 400 s during which the bead achieves a steady reference state of near constant  $Y$  and bead temperature about  $11^\circ\text{C}$  above slab temperature. The laser beam is then blocked for 30 s and then unblocked. This leads to the bead experiencing 30 s of transient cooling. As seen in the figure, the shifts  $Y$  still track the temperature changes. Again one sees that the observed shifts  $Y$  are chiefly due to temperature dependence of elastic moduli in the vicinity of the contact. The quantity  $T_b$  is now negative, as it is still defined as the change in bead temperature relative to its value before the laser beam was blocked. The best fit value for  $\beta$  is unchanged. This rules out, for example, significant losses of stiffness due to bond breaking from tangential sliding due to differential thermal expansion across temperature gradients at the bead-slab contact. Such sliding and breaking would lead to the same loss of stiffness regardless of whether it was caused by cooling or heating.

The conclusion is that transient changes in bead interface stiffness due to temperature largely correspond to the classical effect in which modulus varies linearly and instantaneously with temperature. Heating and cooling make little slow dy-

namic or other nonlinear contributions to  $Y$ . Figure 7 shows that that conclusion is reproduced in further tests.

The changes seen here on heating or cooling are qualitatively different from those observed by Ten Cate *et al.* [27] (Fig. 1 above) who observed immediate stiffness drops and slow recoveries regardless of the sign of temperature change. We can speculate as to the reason. It may be imagined that the behavior seen in sandstone was due to thermal stresses owing to inhomogeneous thermal expansion coefficients, perhaps due to inhomogeneous chemistry or to anisotropic crystallites with inhomogeneous orientations. These thermal stresses would then be expected to lead to SD behavior much as do applied stresses. In the single-bead system, on the other hand, the structure is nominally homogeneous; both slabs and beads are composed of the same material, aluminum, known for not exhibiting SD in the bulk. In addition, aluminum crystallites are cubic with isotropic thermal expansion coefficients, so there are no intercrystallite thermal stresses.

This section has introduced two fitting parameters.  $\beta$  is the observed proportionality between  $T(t)$  and  $Y(t)$ , found to be the same for both heating and cooling, and to be reproducible if the bead is not disturbed. Small deviations from perfect proportionality presumably indicate a degree of SD-like behavior. The other parameter,  $\Delta$ , is a best fit delay between temperature and thermocouple reading, also found to be reproducible and unchanged between heating and cooling. Neither parameter is used below.

## IV. HYBRID TESTS, VIBRATION CONDITIONING FOLLOWED BY TEMPERATURE CHANGES

Because heating induces few SD effects on its own, we are encouraged to investigate how it superposes with vibration-induced SD. Chief among the models for how heating might affect SD recoveries is that of Arrhenius [29,32–35]. The first of the following subsections shows that even small transient temperature changes will, according to Arrhenius, dramatically affect SD recoveries. The second and third subsections present measurements of SD recovery before, during, and af-

ter transient temperature changes. It is found that heating does enhance healing, but the measured enhancement is stronger than predicted by Arrhenius. It is further found that cooling has no discernible effect.

### A. Arrhenius theory

One form of the Arrhenius conjecture, see Bouquet *et al.* [32] or Amir *et al.* [33], posits that slow dynamics recoveries are governed by bond formation due to thermal activation over energy barriers with a distribution of heights. Straightforward calculations show that room temperature  $\log(t)$  recovery may be derived from this Arrhenius conjecture with few additional assumptions. One starts with a relaxing quantity  $F(t)$  (a modulus or a wave speed or a resonant frequency) with time dependence of the form

$$F(t) = F_\infty - \int_0^\infty f_0(E_A) e^{-\nu t \exp(-E_A/kT)} dE_A, \quad (3)$$

where  $T$  is absolute temperature and  $k$  is Boltzmann's constant.  $F_\infty$  is a reference value equal to  $F(t = \infty)$ .  $\nu$  is sometimes called the attack rate.  $f_0$  is a distribution of activation, or barrier, energies  $E_A$ .  $f_0$  must diminish sufficiently quickly at large  $E_A$  for the existence of the integral. (That condition on  $f_0$  may be removed by rewriting (3) in the form  $F(t) = F(t=0) + \int f_0(E_A) \{1 - \exp(-\nu t \exp(-E_A/kT))\} dE_A$ .)

This picture is mathematically equivalent to representing  $F(t)$  as a superposition of exponential relaxations  $\exp(-t/\tau)$  with a distribution in  $\tau$  [8,16,26].

$$F(t) = F_\infty - \int_0^\infty [A(\tau)/\tau] e^{-t/\tau} d\tau,$$

as may be established by changing the integration variable from  $E_A$  to  $\tau$  using  $\tau = \exp(E_A/kT)/\nu$ .  $A(\tau)$  may be termed the relaxation spectrum. This form for  $F(t)$  leads to  $\log(t)$  linearity when  $A$  is constant over wide a range in  $\tau$  [26].

The Arrhenius expression (3) simplifies in an asymptotic limit  $E_A/kT \gg 1$  or alternatively,  $\log(\nu t) \gg 1$  (well satisfied for the times of interest in SD experiments and for the usual identification of  $\nu$  with  $10^{12}/s$ ). In this case the exponential in Eq. (3) approximates to a Heaviside step function  $\exp[-\nu t \exp(-E_A/kT)] \approx \Theta[kT \ln(\nu t) - E_A]$ . Equation (3) then becomes

$$F(t) = F_\infty - \int_{kT \ln(\nu t)}^\infty f_0(E_A) dE_A.$$

Its time derivative is evaluated to be

$$dF(t)/d \ln(t) = kT f_0[kT \ln(\nu t)], \quad (4)$$

thereby showing that  $F$  is linear in  $\log(t)$  whenever  $f_0(E_A)$  is constant. A more detailed treatment (see the Appendix) without asymptotic assumptions derives (4), but with the right side replaced with  $f_0$  smoothed over a range of order  $kT$ , thus predicting linearity in  $\log(t)$  under the less restrictive condition: whenever the *smoothed*  $f_0$  is constant.

The thermal activation conjecture thus replaces the mystery of  $\log(t)$  recovery over decades of time, or the constancy of  $A(\tau)$  over decades in  $\tau$ , with a less mysterious hypothesis of a flat distribution,  $f_0(E_A) = \text{constant}$ , over a short range of activation energies. Indeed, a constant slope  $dF/d \ln(t)$  from

1 s to 20 min, i.e., over three orders of magnitude in time, requires merely (we take  $\nu$  to be the conventional  $10^{12}/s$  though the precise value is unimportant) that  $f_0(E_A)$  be constant from  $E_A = 0.69$  to  $0.86$  eV. The hypothesis is attractive in that it naturally predicts  $\log(t)$  recoveries over orders of magnitude of time, requiring constancy of  $f_0$  over only short ranges of activation energy.

In spite of its apparent naturalness and the ease with which it predicts  $\log(t)$  recoveries, the thermal activation conjecture for slow dynamic recovery of stiffness has not been confirmed in the laboratory. TenCate *et al.* [1] attempted confirmation by studying stiffness loss and healing at different temperatures. The conjecture predicts [Eq. (4)] that  $F$ 's slope with respect to  $\log(t)$  ought to be proportional to absolute temperature. They were unable to observe that. This may have been because the Arrhenius conjecture is incorrect. Alternatively, one could ascribe the result to their inability to control for the temperature dependence of the amount of initial stiffness loss  $\int f_0(E_A) dE_A$  induced by their mechanical conditioning. They were further hampered by access to only a limited temperature range imposed by their apparatus and by a desire not to bake the constitutive clays.

Single-bead experiments with laser heating permit an alternate protocol, one in which temperature is quickly raised or lowered during a recovery. As shown below, such transient heating can amplify temperature sensitivity beyond that predicted in Eq. (4). If the temperature changes occur after the mechanical conditioning, the initial stiffness diminishment from the mechanical conditioning is unaffected, and if the Arrhenius conjecture is correct, the recovery accelerates (decelerates) significantly when the temperature increases (decreases). This is illustrated by solutions to the following equations governing recovery from mechanical conditioning while temperature is time varying.

$$\begin{aligned} f(E_A, 0) &= f_0(E_A), \\ df(E_A, t)/dt &= -f(E_A, t) \nu \exp[-E_A/kT(t)], \end{aligned} \quad (5)$$

$$F(t) = F_\infty - \int_0^\infty f(E_A, t) dE_A.$$

An initial density  $f_0(E_A)$  of barrier heights depletes according to the Arrhenius law at a rate that depends on temperature. When applied to the single-bead system of Fig. 2,  $T$  must be identified with the temperature  $T_i$  at the interface, not the temperature of the bead. Equations (3) and (4) are recovered if  $T$  is constant.

Equation (5) was integrated numerically under three different  $T(t)$  protocols. The initial distribution  $f_0$  was taken to be uniform from 0 to 1.5 eV.  $\nu$  was taken to be  $10^{12}/s$ . The resulting recoveries  $F(t) - F_0$  are displayed in Fig. 8 in arbitrary units vs  $\ln(t/s)$ . The straight line is the predicted behavior for constant 293 K temperature and shows the familiar linearity in  $\log(t)$ . The upper crooked line is for the case in which absolute interface temperature was raised by 2%, from 293 to 299 K (corresponding to absolute bead temperature raised 4% from 293 to 305 K as in Fig. 4, i.e.,  $T_b$  being raised by 12 K) 20 s after the recovery began, and held there for 30 s before being quickly brought back. The difference between the straight and upper crooked lines is striking and should be detectable given sufficient measurement precision. During

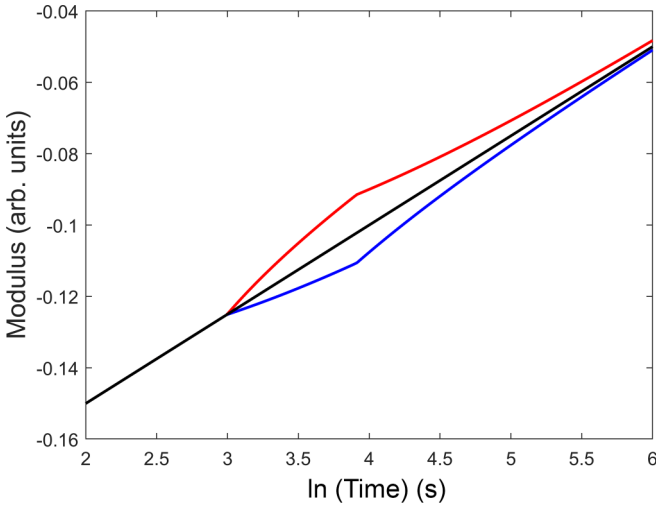


FIG. 8. Predicted SD recoveries (in arbitrary units and shifted arbitrarily) vs  $\ln(t/s)$  according to the Arrhenius conjecture, Eq. (5), with an assumed uniform distribution of activation energies. The straight black line is for a fixed absolute temperature of 293 K. The two crooked lines are for an initial temperature of 293 K followed by, after 20 s, 30 s of a, respectively, 2% higher (red, upper line) or lower (blue, lower line) temperature.

the 30 s of 2% higher absolute temperature, the recovery was accelerated by far more than 2%. During the 30 s period of enhanced temperature, energy barriers  $E_A$  were overcome that would have required 57 s if  $T$  had not been briefly boosted. The average healing rate has nearly doubled. Recovery is slower after recooling and asymptotes back onto the original linearity in  $\log(t)$ . The figure also shows the predicted effect of a 2% absolute temperature drop, from 293 to 287 K for 30 s. As with the response to heating, the change in slope is far more than 2%.

Baumberger and Caroli [34], Brechet and Estrin [35], and Lebedev and Ostrovky [29] offer an alternative Arrhenius argument for  $\log(t)$  recovery. If the load on the contact area is fixed then the stress will diminish as the area grows  $\sigma \propto (\text{Area})^{-1}$ . They take that area growth to be plastic and governed by an Arrhenius rule of the form  $dA/dt \propto \exp(-\sigma V/kT)$  where  $V$  is a relevant activation volume for the plastic flow. On assuming SD stiffness  $F$  is a linear proxy for contact area, and that changes in area are small and may be linearized, one recovers a differential equation governing the SD recovery:  $dF/dt \propto \exp(-F/kT)$ , whose solution is linear in  $\log(t)$ . Numerical solutions of this model reproduce Fig. 8 with high precision. In particular, this model exhibits the same striking amplification of small temperature changes as does Eq. (5).

Taking  $\nu$  at a nonphysical value much greater than  $10^{12}$  enhances the effect of transient temperature changes. For example, the choice,  $\nu = 10^{18}$ , leads to the crooked lines becoming about 50% further from the straight line.

**B. Hybrid tests, heating**

Figure 9 shows the shifts for a hybrid measurement of shift  $Y$ , here called  $H(t)$ , that combines vibration conditioning and transient heating. After a rest period of 1 h or more,

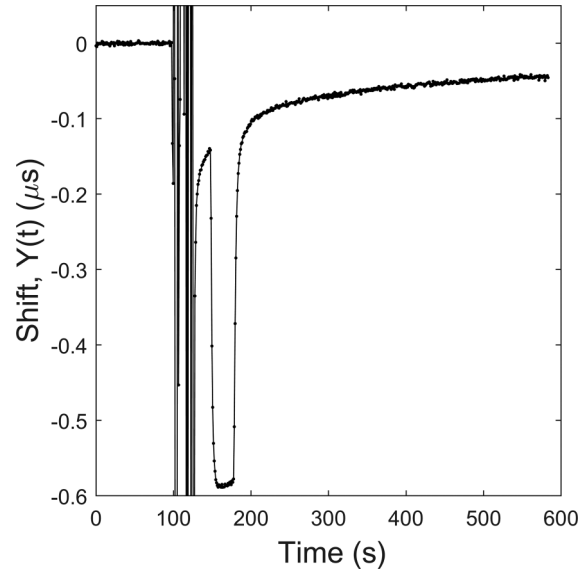


FIG. 9.  $H(t)$ , the shift  $Y$  in a hybrid test in which vibration conditioning is followed by 20 s of free recovery and then 30 s of laser heating and then further recovery.

coda-wave-interferometric monitoring began at  $t = 0$ . Vibration conditioning was then applied between times  $t = 100$  and  $t = 130$  s. Recovery commenced at  $t = 130$  s but was interrupted at  $t = 150$  s by 30 s of laser heating, after which the recovery was monitored for another 400 s. Figure 10 shows the same data vs  $\log(t)$ .

Until 20 s after vibration cessation, recovery proceeds linearly with  $\log(t)$ , as may be seen in Fig. 10. Later, between 20 and 50 s after cessation, i.e., during the period of elevated bead temperature, shifts  $Y$  are dominated by loss of stiffness due to heating. At late times, after the temperature drops again,

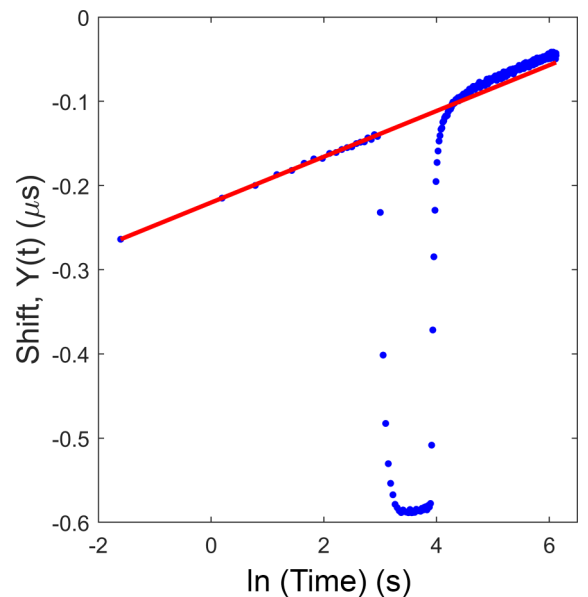


FIG. 10. The hybrid data  $H(t)$  of Fig. 9 are plotted vs  $\log(t)$ . Measured shifts in blue dots. A linear extrapolation of early behavior is shown in the straight red line.



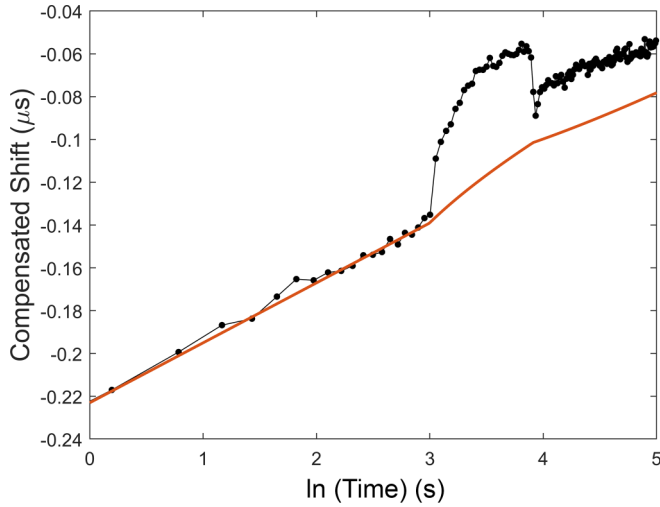


FIG. 11. Compensated shift  $C = H - L$ , black dots, where  $H$  is the hybrid test's shifts as in Fig. 10, and  $L$  is the unattenuated laser-alone shift as in Fig. 5. The solid line is the Arrhenius prediction, Fig. 8, for the case  $\nu = 10^{12}/\text{s}$  and a 2% temperature increase. This plot illustrates a spike and step discontinuity at laser-off ( $\ln t = 3.9$ ) due, respectively, to imperfect temporal alignment of  $L$  and  $H$ , and the failure to attenuate  $L$  before subtraction.

the recovery asymptotes to a line parallel with the original trend, but shifted vertically by about 10 ns, indicating that the heating has had a net effect of increasing contact stiffness by a small amount. The heating has healed the system over and above the healing it would have achieved on its own. That much is consistent with the Arrhenius hypothesis, but the predicted increased healing (Fig. 8) asymptotes toward the original trend, while the measured seems to parallel the original trend. The discrepancy is even greater when one recalls, Figs. 5 and 7, that heating alone would have degraded system stiffness.

While Fig. 10's behavior after laser-off shows failure of the Arrhenius conjecture, the loss of stiffness due to heating has obscured the full record of stiffness recovery, most seriously while the laser is on. In order to separate the direct effects of the heating and discern any effect on the SD healing while the laser is on, we subtract from  $H(t)$  the laser-alone shifts  $L(t)$ , where  $L$  is the  $Y(t)$  measured during transient heating of the same undisturbed bead (and shifted in time to align the times of laser-on and -off.) A typical  $L(t)$  with no time shifting was seen in Fig. 5.  $L(t)$  for the subtraction is measured some 30 min after  $H$ , without disturbing the bead.

Removal of the direct effects of the heating is a delicate process. Figure 11 shows a compensated shift  $C(t) = H(t) - L(t)$  with two unphysical features. Insufficient precision in doing the temporal alignment has led to a delta-function-like spike at the time ( $\ln t = 3.9$ ) of laser-off. This spike disappears if greater care is taken in doing temporal alignments. Figure 11 also shows an unphysical step discontinuity of about 20 ns at the time of laser-off. This step discontinuity disappears if the laser-alone shifts  $L$  are attenuated before subtraction. The appropriateness of such attenuation could have been expected. Recall that shifts  $Y$  are affected by the ultrasonic loss rate  $\gamma$  in the bead [Eq. (2)], which are in turn

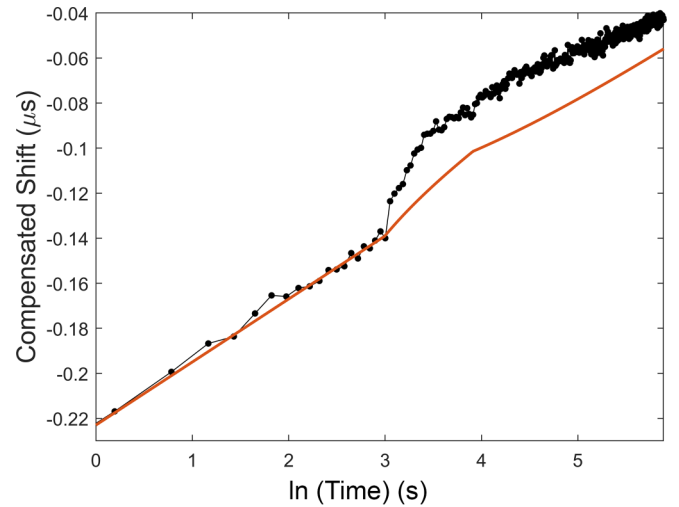


FIG. 12. Compensated shift  $C = H - (1-p)L$ , with  $p$  chosen at 5% and greater care in the temporal alignment. The delta-function-like spike and the step discontinuity that appeared in Fig. 11 at  $\ln(t) = 3.9$  have been eliminated.

affected by the SD loss of stiffness [Eq. (1)]. We put these together and predict that  $L$  ought to be replaced by  $(1-p)L$ , with  $p = -\gamma_{\text{SD}}\omega Y/R$ . Unfortunately  $R$  and  $\gamma_{\text{SD}}$  are known only approximately, but  $p$  can be roughly estimated as 0.026 using  $Y = -120$  ns,  $\gamma_{\text{SD}} = 0.35$ , and  $R = 1$ .

Figures 12 and 13 show compensated shifts  $C(t) = H(t) - (1-p)L(t)$ . A spline like algorithm [42] is used to interpolate the data and align time stamps in order to eliminate spike discontinuities like that in Fig. 11. Figure 11's step discontinuity at  $\ln(t) = 3.9$  has been eliminated by using an attenuation  $p$  with a value that best does this, a value consistent with the prediction that  $p$  is of order 2.6%. The behavior shown in these figures is not as Arrhenius would have it. The plot shows that healing has been accelerated by the raised temperature, but more than predicted. As observed

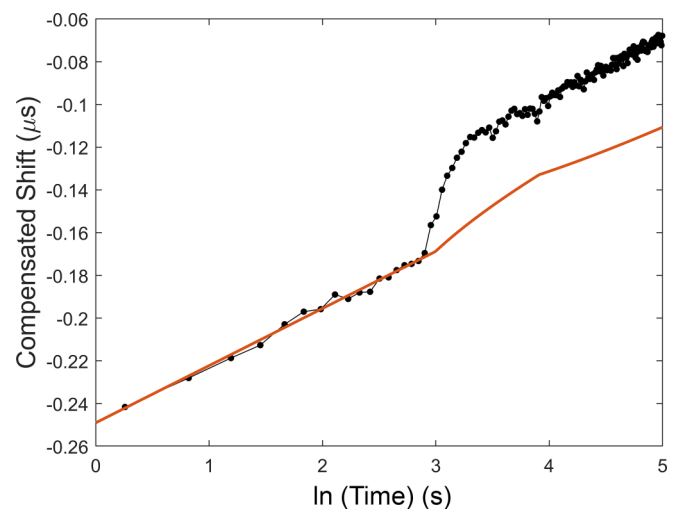


FIG. 13. Compensated shift  $C = H - (1-p)L$  for a separate test, but with identical protocol.  $p$  is chosen at 4%. The disagreement with the Arrhenius prediction is greater than in Fig. 12.

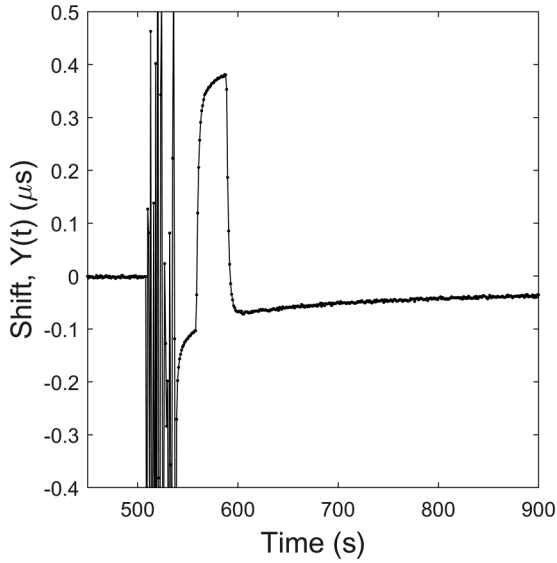


FIG. 14. Hybrid shift  $H(t)$  for the case of 30 s of lower temperature.

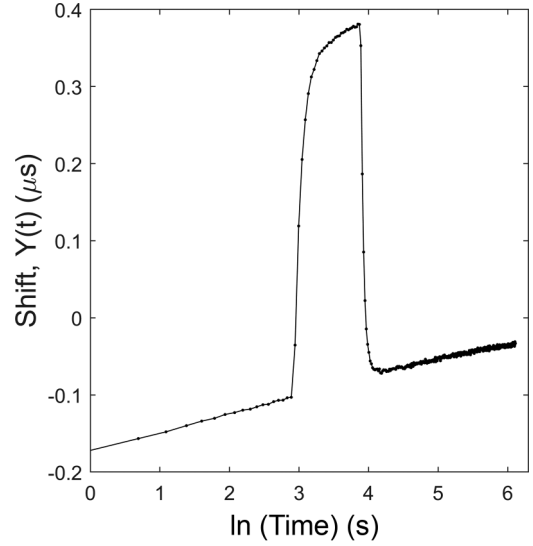


FIG. 15. The data  $H(t)$  of Fig. 14, plotted vs  $\ln(t)$ .

in the discussion following Fig. 10, the difference between theory and measurement at very late times remains higher than the Arrhenius prediction, about 15 ns in Fig. 12 and 40 ns in Fig. 13.

**C. Hybrid tests, cooling**

We also examine the effect on SD healing of a short period of cooling. The test protocol consists of 500 s of laser illumination to bring the bead into a steady state at an elevated temperature about 11°C above the slabs. A 30 s period of vibration conditioning was then applied while maintaining the illumination. A curious 1°C further increase of temperature (not shown) occurs during the vibration and is attributed to a vibration-induced drop in time-averaged thermal conductance. (Vibration alone does not noticeably raise bead temperature.) Vibration ceases after 30 s but laser illumination continues with the temperature dropping back by the curious 1°C to its value before vibration. At this point the system is essentially equivalent to the standard test, e.g., Fig. 3, but at an elevated temperature. Twenty seconds after the vibration turns off, the laser beam is blocked for 30 s, causing the temperature to drop. The laser is then unblocked and the recovery monitored for another 300 s. This is equivalent to the standard test, though at elevated initial temperature and with a 30 s period of transient cooling imposed 20 s after vibration conditioning.

The resulting hybrid shift is shown in Fig. 14. The initial recovery from 530 to 550 s is followed at 550 s by a large step up due to the cooling, followed by a step down at 580 s upon reheating. Thereafter  $H$  continues to slowly recover. A second cooling, 30 min later (not shown), allows us to assess the effect of cooling alone, as in Fig. 6.

In Fig. 15 the same data are displayed vs  $\log(t)$ . It shows the usual linearity, though interrupted by the cooling. After the period of lower temperatures ends, the recovery resumes, and on a line very nearly identical to an extrapolation of the

early time recovery. The cooling seems to have had no long term effect.

As previously, we can subtract the profile of the cooling alone from the hybrid data of Figs. 14 and 15 to recover what  $Y$  would be without the modulus changes due to the cooling. The result is shown in Figs. 16 and 17.  $p$  was taken to be 1% and 1.1%, respectively.

Figures 16 and 17 of compensated shift  $H-(1-p)L$  show no clear sign of the predicted (Fig. 8) Arrhenius behavior. Cooling has had no clear effect. The disagreement with Arrhenius is less severe than it was in Figs. 11 and 12 for transient heating, but it remains discernible, peaking at 13 and 9 ns, respectively.

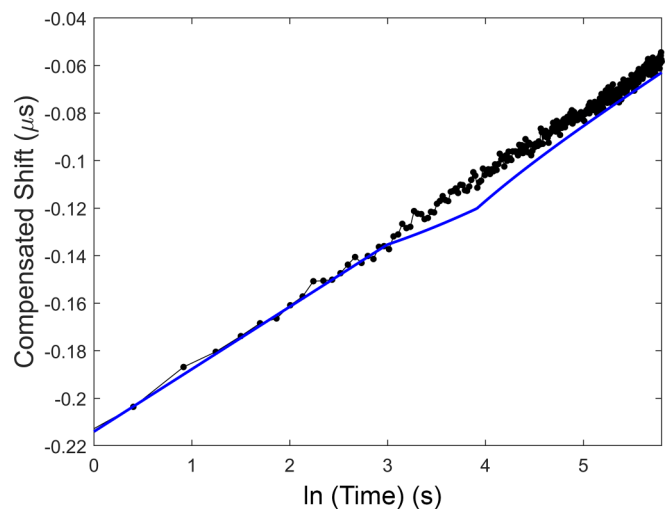


FIG. 16. Compensated shift  $C(t) = H(t)-(1-p)L(t)$  for the case of 30 s of cooling is compared with theory (Fig. 7) for  $\nu = 10^{12}/s$ .  $p$  is chosen at 1%.

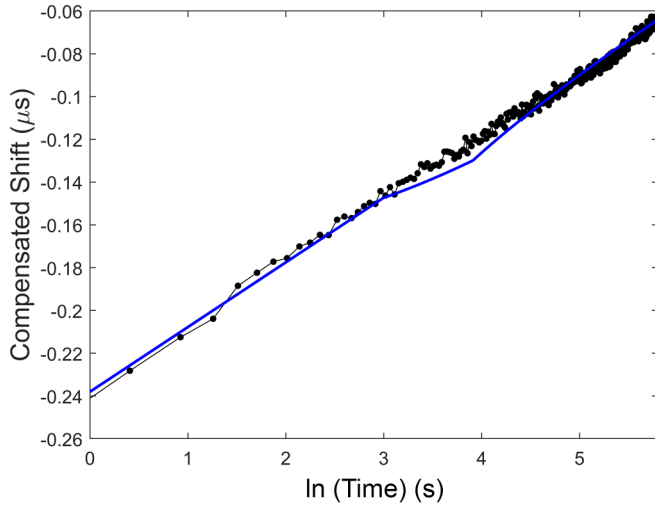


FIG. 17. Compensated shift  $C(t) = H - (1-p)L$  for a separate measurement of the response to transient cooling. Protocol is identical to that of Fig. 16.  $p = 1.1\%$ .

#### D. Interpretation

The fitting parameters  $t_0$ ,  $\beta$ , and  $\Delta$  introduced in Secs. II and III do not affect the construction of  $C(t)$  so the conclusions below are not dependent upon them. In Secs. IV B and IV C the choice of time shift to be applied to  $L$  before subtraction from  $H$  is also unimportant; doing so removes an unphysical spike in  $C(t)$  but the effect is local and not determinative in the conclusions below. The parameter  $p$  representing the attenuation to be applied to  $L(t)$  before subtraction from  $H(t)$  is arguably more *ad hoc* and consequential. It was chosen to eliminate step discontinuities like that illustrated in Fig. 11 and that we judge to be unphysical. If it had not been applied, however, the discrepancy with Arrhenius would be more severe and more complex, so our qualitative conclusions would be unchanged.

The compensated plots  $C = H - (1-p)L$  could differ from linear extrapolation of their early times for either of two reasons. (1) The changed temperatures may affect the SD recovery from the vibrations; indeed, this is what we wish to detect in general, with particular interest in seeing whether or not that effect is consistent with the Arrhenius conjecture, Eq. (5). One must also consider the possibility (2) that the stiffness loss associated with transient temperature changes might be enhanced or diminished when concurrent with an ongoing SD recovery. Stiffness loss associated with heating or cooling and which is unaffected by concurrent SD recovery from mechanical conditioning (for example, that due to temperature-dependent moduli) does not meet the latter possibility. To meet the possibility one must imagine that heating during the hybrid  $H(t)$  does more, or less, damage than does heating in the reference measurement  $L(t)$ . Inasmuch as  $L$  exhibits very little damage (Figs. 5–7), this may be difficult to maintain. One way to envision how the heating in a hybrid test may be doing less damage than the reference heating in  $L$  is to imagine that there are bonds that are broken during laser-alone measurements, breakages that contribute to loss of

stiffness beyond that encompassed by  $\beta T$  and apparent at late times in Figs. 5–7. Some of these same bonds may also have been broken by the mechanical conditioning in the hybrid tests. If they remain as yet unhealed at the time of the heating in the hybrid tests then the laser is incapable of breaking these bonds, because they are already broken. This implies that the  $L(t)$  used to compensate would be reporting more damage than it should. The possibility is intriguing and has the right sign to reconcile Arrhenius with  $C(t)$ , as it makes the compensated  $C(t)$  less healed, but the effect is small. It is too small, for example, to explain the 15 ns discrepancy at late times in Fig. 12, or the 40 ns discrepancy at late times in Fig. 13. The other hypothesis, that the laser might do more damage on the partially healed system than it does when acting on its own, has the wrong sign to reconcile Arrhenius with  $C(t)$ .

The conclusion is that the Arrhenius conjecture, Eq. (5), is not supported by the measurements. During the period of transient heating (Figs. 9–13) the rate of healing is indeed increased, but in excess of predictions. Nevertheless, the measured changes in healing are of the same order as the Arrhenius prediction, which suggests that Arrhenius may be approximately correct and that minor considerations might suffice to improve the match with measurements. Positing super-Arrhenius kinetics is one possibility. Such are apparently common in complex processes when consecutive reactions contribute [43]. The literature’s more extreme quotes [44] for  $dE_A/dT$  may be sufficient to reconcile some of Figs. 9–13 with a generalized Arrhenius picture. This may be seen if we take effective activation energy of a bond to be temperature dependent, e.g.,  $E_{\text{Aeff}} = E_0 - \zeta kT$ . Then the rate factor  $\nu \exp(-E/kT)$  in Eq. (5) becomes  $\nu \exp(-E_{\text{Aeff}}/kT) = \nu \exp(\zeta) \exp(-E_0/kT)$ . For large positive  $\zeta$ , this is mathematically equivalent to a significantly increased attack rate, and as remarked in Sec. IV A, will accelerate the predicted healing above that of the upper (red) line in Fig. 8 and bring theory into better agreement with measurements.

Positing super-Arrhenius kinetics does not, however, help in reconciling theory with the data after the temperature has fallen again,  $t > 50$  s after vibration cessation. Theory, regardless of the effective  $\nu$ , predicts healing to slow and asymptotically approach the original line (Fig. 8). Yet the measurements show healing to continue, with a constant slope.

Nor does positing super-Arrhenius kinetics reconcile theory with the measurements for transient cooling where Figs. 16 and 17 do not exhibit the predicted slowing of healing

It is also worth considering that the value of attenuation  $p$  used to construct  $C = H - (1-p)L$  and eliminate the step discontinuity may have been incorrect. While there must be some  $p$  of the order of a few percent, we have no independent way of accurately estimating it. One can imagine that perhaps some of that discontinuity seen in Fig. 11 represents part of the physics at cooling and ought not have been artificially removed. Perhaps the step down discontinuity at laser-off in Fig. 11 includes damage on cooling. This requires a picture in which sudden cooling does more damage to bonds that are recently healed than to those that are fully healed. It is not impossible to subscribe to such a multiplication of hypotheses, but even if one does, it leaves us with Fig. 11’s even greater difference between measurements and Arrhenius prediction before laser-off.

**V. SUMMARY**

It has been found that transient heating or cooling of the single aluminum bead system without mechanical conditioning leads to little or no long term modulus loss or SD recovery. This system’s change of stiffness upon heating and cooling alone is dominated by the familiar classical instantaneous temperature-dependent material moduli. This is in contrast to reports elsewhere of SD behavior after transient heating or cooling in sandstone.

Hybrid tests are conducted also, in which SD recoveries from mechanical conditioning are combined with transient heating and cooling. Such tests permit investigation of the Arrhenius conjecture that SD healings are governed by thermally activated barrier hopping over a distribution of barrier heights. Numerical calculations show that Arrhenius predicts strong healing rate changes even when absolute temperature changes are as little as 2%. After doing such tests, and subtracting the effect of heating alone, we find that the Arrhenius conjecture is not supported. While the compensated recovery profiles in Figs. 12 and 13, and 16 and 17 do not differ enormously from the predicted, they do so to a degree well above the apparent noise.

While a simple Arrhenius picture is rejected, the data do not demand more general rejection. Indeed, that the measured changes in healing are of the same order as the Arrhenius prediction suggests that Arrhenius is approximately correct and that minor variations in theory, or hypotheses of additional mechanisms, might suffice to improve the match with measurements. One might, for example, consider the literature on super-Arrhenius kinetics [43,44].

Further tests are indicated. The obvious ones would be tests with materials other than aluminum.

**ACKNOWLEDGMENTS**

The authors are grateful to J. Yoritomo for his original development of the experimental system, and for discussions. The work was supported by the U.S. Department of Energy, Office of Science, Office of Basic Energy Sciences, under Award No. DE-SC0021056.

**APPENDIX: DERIVATION OF log(t) LINEARITY FROM THE ARRHENIUS HYPOTHESIS EQUATION (3)**

We replace the lower limit in Eq. (3) with  $-\infty$ , with the understanding that  $f_0$  vanishes for negative  $E_A$ . We also change variables:  $E_A = kT(\ln vt + q)$ ;  $dE_A = kT dq$ , and derive

$$F(t) = F_\infty - kT \int_{-\infty}^{\infty} f_0[kT(\ln vt + q)] e^{-\exp(-q)} dq. \quad (A1)$$

Taking the derivative  $d/d \ln t = d/d \ln vt$  and replacing  $d/d \ln vt$  acting on  $f_0$  with  $d/dq$  acting on  $f_0$ , we obtain

$$\begin{aligned} dF(t)/d \ln t \\ = -kT \int_{-\infty}^{\infty} \{df_0[kT(\ln vt + q)]/dq\} e^{-\exp(-q)} dq. \end{aligned} \quad (A2)$$

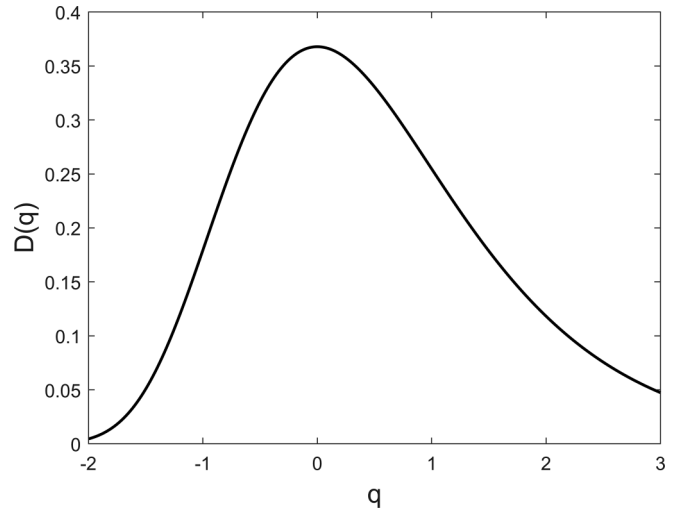


FIG. 18. The weighting function  $D(q)$  appearing in Eq. (A3).

On integrating by parts [and remembering  $f_0(\infty) = 0$ , required for the existence of Eq. (3)] we have

$$\begin{aligned} dF(t)/d \ln t &= kT \int_{-\infty}^{\infty} f_0[kT(\ln vt + q)] \frac{d\{e^{-\exp(-q)}\}}{dq} dq \\ &= kT \int_{-\infty}^{\infty} f[kT(\ln vt + q)] e^{-q-\exp(-q)} dq \\ &= kT \int_{-\infty}^{\infty} f_0[kT(\ln vt + q)] D(q) dq = kT \langle f_0 \rangle. \end{aligned} \quad (A3)$$

The above integral describes a weighted average of  $f_0$  over a region near  $q = 0$ . The weighting function  $D(q) = \exp[-q-\exp(-q)]$  is zero for large positive or negative  $q$ . It peaks at  $q = 0$  with a value of  $1/e$ . The area under the curve is unity. Mean  $q$  is  $\gamma = 0.577$ ; standard deviation is  $\pi/\sqrt{6} = 1.28$ .  $D(q)$  is plotted in Fig. 18.

We conclude

$$dF/d \ln t = kT \langle f_0 \rangle, \quad (A4)$$

with the brackets indicating a smoothly weighted average of  $f_0$  over a short range of order  $kT$  in the vicinity of  $E_A = kT \ln(vt)$ .

In the asymptotic limit  $kT \ll E_A$ , or  $vt \gg 1$ ,  $D(q)$  becomes a delta function, and Eq. (A4) becomes  $dF/d \ln t = kT f_0[kT \ln(vt)]$ , without the brackets  $\langle \dots \rangle$ .



- [1] J. A. TenCate, E. Smith, and R. A. Guyer, Universal Slow Dynamics in Granular Solids, *Phys. Rev. Lett.* **85**, 1020. (2000).
- [2] J. A. Ten Cate and T. J. Shankland, Slow dynamics in the nonlinear elastic response of Berea sandstone, *Geophys. Res. Lett.* **23**, 3019 (1996).
- [3] E. Smith and J. A. TenCate, Sensitive determination of nonlinear properties of Berea sandstone at low strains, *Geophys. Res. Lett.* **27**, 1985 (2000).
- [4] J. A. TenCate, Slow dynamics of earth materials: An experimental overview, *Pure Appl. Geophys.* **168**, 2211 (2011).
- [5] R. A. Guyer and P. A. Johnson, Nonlinear mesoscopic elasticity: Evidence for a new class of materials, *Phys. Today* **52**(4), 30 (1999).
- [6] P. A. Johnson and A. Sutin, Slow dynamics and anomalous fast dynamics in diverse solids, *J. Acoust. Soc. Am.* **117**, 124 (2005).
- [7] R. A. Guyer and P. A. Johnson, *Nonlinear Mesoscopic Elasticity* (Wiley, Weinheim, 2009).
- [8] P. Shokouhi, J. Riviere, R. Guyer, and P. A. Johnson, Slow dynamics of consolidated granular systems: Multi-scale relaxation, *Appl. Phys. Lett.* **111**, 251604 (2017).
- [9] O. I. Lobkis and R. L. Weaver, On the Larsen effect to monitor small fast changes in materials, *J. Acoust. Soc. Am.* **125**, 1894 (2009).
- [10] D. P. Schaff and G. C. Beroza, Coseismic and postseismic velocity changes measured by repeating earthquakes, *J. Geophys. Res.: Solid Earth* **109**, B10302 (2004).
- [11] F. Brenguier, M. Campillo, C. Hadziioannou, N. M. Shapiro, R. M. Nadeau, and E. Larose, Postseismic relaxation along the San Andreas Fault at Parkfield from continuous seismological observations, *Science* **321**, 1478 (2008).
- [12] M. Gassenmeier, C. Sens-Schonfelder, T. Eulenfeld, M. Bartsch, P. Victor, F. Tilmann, and M. Korn, Field observations of seismic velocity changes caused by shaking-induced damage and healing due to mesoscopic nonlinearity, *Geophys. J. Int.* **204**, 1490 (2016).
- [13] M. Scalerandi, C. Mechri, M. Bentahar, A. Di Bella, A. S. Gliozzi, and M. Tortello, Experimental Evidence of Correlations between Conditioning and Relaxation in Hysteretic Elastic Media, *Phys. Rev. Appl.* **12**, 044002 (2019).
- [14] N Tremblay, E. Larose, and V. Rossetto, Probing slow dynamics of consolidated granular multicomposite materials by diffuse acoustic wave spectroscopy, *J. Acoust. Soc. Am.* **127**, 1239 (2010).
- [15] A Astorga, P. Guéguen, and T. Kashima, Nonlinear elasticity observed in buildings during a long sequence of earthquakes, *Bull. Seismol. Soc. Am.* **108**, 1185 (2018).
- [16] J. Kober, A. S. Gliozzi, M. Scalerandi, and M. Tortello, Material Grain Size Determines Relaxation-Time Distributions in Slow-Dynamics Experiments, *Phys. Rev. Appl.* **17**, 014002 (2022).
- [17] J. A. Bittner, Understanding and predicting transient material behaviors associated with mechanical resonance in cementitious composites, Ph.D. thesis, University of Illinois, Urbana-Champaign, 2019.
- [18] J. A. Bittner and J. S. Popovics, Direct imaging of moisture effects during slow dynamic nonlinearity, *Appl. Phys. Lett.* **114**, 021901 (2019).
- [19] V. Zaitsev, V. Gusev, and B. Castegnede, Thermoelastic Mechanism for Logarithmic Slow Dynamics and Memory in Elastic Wave Interactions with Individual Cracks, *Phys. Rev. Lett.* **90**, 075501 (2003).
- [20] P. A. Johnson and X. Jia, Nonlinear dynamics, granular media and dynamic earthquake triggering, *Nature* **437**, 871 (2005).
- [21] V. Zaitsev, V. Gusev, V. Tournat, and P. Richard, Slow Relaxation and Aging Phenomena at the Nanoscale in Granular Materials, *Phys. Rev. Lett.* **112**, 108302 (2014).
- [22] X. Jia, T. Brunet, and J. Laurent, Elastic weakening of a dense granular pack by acoustic fluidization: Slipping, compaction and aging, *Phys. Rev. E* **84**, 020301(R) (2011).
- [23] J. Y. Yoritomo and R. L. Weaver, Slow dynamic nonlinearity in unconsolidated glass bead packs, *Phys. Rev. E* **101**, 012901 (2020).
- [24] J. Y. Yoritomo and R. L. Weaver, Slow dynamics in a single glass bead, *Phys. Rev. E* **101**, 012902 (2020).
- [25] J. Y. Yoritomo and R. L. Weaver, Slow dynamic elasticity in unconsolidated metal structures, *Phys. Rev. E* **102**, 012901 (2020).
- [26] R. Snieder, C. Sens-Schonfelder, and R. Wu, The time dependence of rock healing as a universal relaxation process, a tutorial, *Geophys. J. Int.* **208**, 1 (2016).
- [27] J. A. Ten Cate, J. J. Duran, and T. J. Shankland, Nonlinearity and slow dynamics in rocks: Response to changes of temperature and humidity, in *Nonlinear Acoustics at the Beginning of the 21st Century*, edited by O. V. Rudenko and O. A. Sapozhnikov (Faculty of Physics, MSU Press, Moscow, 2002), Vol. 2, pp. 767–770.
- [28] G. Renaud, J. Riviere, P.-Y. Le Bas, and P. A. Johnson, Hysteretic nonlinear elasticity of Berea sandstone at low-vibrational strain revealed by dynamic acousto-elastic testing, *Geophys. Res. Lett.* **40**, 715 (2013).
- [29] A. V. Lebedev and L. A. Ostrovsky, A unified model of hysteresis and long-time relaxation in heterogeneous materials, *Acoust. Phys.* **60**, 555 (2014).
- [30] C. Sens-Schoenfelder, R. Snieder, and X. Li, A model for nonlinear elasticity in rocks based on friction of internal interfaces and contact aging, *Geophys. J. Int.* **216**, 319 (2019).
- [31] L. Gao, P. Shokouhi, and J. Riviere, Effect of relative humidity on the nonlinear elastic response of granular media, *J. Appl. Phys.* **131**, 055101 (2022).
- [32] L. Bouquet, E. Charlaix, S. Ciliberto, and J. Crassous, Moisture-induced ageing in granular media and the kinetics of capillary condensation, *Nature (London)* **396**, 735 (1998).
- [33] A. Amir, Y. Oreg, and Y. Imry, On relaxation and aging of various glasses, *Proc. Natl. Acad. Sci. USA* **109**, 1850 (2012).
- [34] T. Baumberger and C. Caroli, Solid friction from stick-slip down to pinning and aging, *Adv. Phys.* **55**, 279 (2006).
- [35] Y. Brechet and Y. Estrin, The effect of strain rate sensitivity on dynamic friction of metals, *Scr. Metall. Mater.* **30**, 1449 (1994).
- [36] R. Snieder, A. Gret, H. Douma, and J. Scales, Coda wave interferometry for estimating nonlinear behavior in seismic velocity, *Science* **295**, 2253 (2002).
- [37] R. L. Weaver and S. Lee, Diffuse energy transport and coda-wave interferometry for resonant transmission between reverberant structures, *J. Acoust. Soc. Am.* **150**, 830 (2021).
- [38] K. L. Johnson, *Contact Mechanics* (Cambridge University Press, Cambridge, 1985).

- [39] B. B. Mikic, Thermal contact conductance; theoretical considerations, *J. Heat Mass Transfer* **17**, 205 (1974).
- [40] H. M. Hashemian, K. M. Petersen, D. W. Mitchell, and D. D. Beverly, *In situ* response time testing of thermocouples, *ISA Trans.* **29**, 97 (1990).
- [41] R. McLellan and T. Ishikawa, The elastic properties of aluminum at high temperatures, *J. Phys. Chem. Solids* **48**, 603 (1987).
- [42] H. Akima, A new method of interpolation and smooth curve fitting based on local procedures, *J. ACM* **17**, 589 (1970).
- [43] V. H. Carvalho-Silva, N. D. Coutinho, and V. Aquilanti, Temperature dependence of rate processes beyond Arrhenius and Eyring: Activation and transitivity, *Front. Chem.* **7**, 380 (2019).
- [44] J. R. Hulett, Deviations from the Arrhenius equation, *Q. Rev. Chem. Soc.* **18**, 227 (1964).